

DFT Study of the Interaction of a single Palladium Atom with γ-Alumina Surfaces: the Role of Hydroxylation

M. Corral Valero, M. Digne, P. Sautet, P. Raybaud

▶ **To cite this version:**

M. Corral Valero, M. Digne, P. Sautet, P. Raybaud. DFT Study of the Interaction of a single Palladium Atom with γ-Alumina Surfaces: the Role of Hydroxylation. Oil & Gas Science and Technology - Revue d'IFP Energies nouvelles, 2006, 61 (4), pp.535-545. 10.2516/ogst:2006024a . hal-02005850

HAL Id: hal-02005850
https://ifp.hal.science/hal-02005850

Submitted on 4 Feb 2019

HAL is a multi-disciplinary open access archive for the deposit and dissemination of scientific research documents, whether they are published or not. The documents may come from teaching and research institutions in France or abroad, or from public or private research centers.

L'archive ouverte pluridisciplinaire **HAL**, est destinée au dépôt et à la diffusion de documents scientifiques de niveau recherche, publiés ou non, émanant des établissements d'enseignement et de recherche français ou étrangers, des laboratoires publics ou privés.

Oil & Gas Science and Technology – Rev. IFP, Vol. 61 (2006), No. 4, pp. 535-545
Copyright © 2006, Institut français du pétrole

IFP International Conference
Rencontres scientifiques de l'IFP

Research Advances in Rational Design of Catalysts and Sorbents
Avancées de la recherche dans la conception rationnelle de catalyseurs et d'adsorbants

DFT Study of the Interaction of a single Palladium Atom with γ-Alumina Surfaces: the Role of Hydroxylation

M. Corral Valero[1,2], M. Digne[3], P. Sautet[2] and P. Raybaud[1]

1 Institut français du pétrole, Direction Chimie et Physico-chimie Appliquées, 1 et 4, avenue de Bois-Préau, 92852 Rueil-Malmaison Cedex - France
2 Laboratoire de Chimie, UMR CNRS 5182, École Normale Supérieure de Lyon, 46, allée d'Italie, 69364 Lyon Cedex 07 - France
3 IFP-Lyon, Direction Physique et Analyse, BP 3, 69369 Vernaison - France
e-mail: manuel.corral.valero@ens-lyon.fr - mathieu.digne@ifp.fr - philippe.sautet@ens-lyon.fr - pascal.raybaud@ifp.fr

Résumé — Étude DFT de l'interaction d'un atome de palladium avec les surfaces d'alumine-γ : rôle de l'hydroxylation — Étant donné le rôle important de l'alumine-γ comme support de nombreuses phases actives en catalyse hétérogène, une description améliorée à l'échelle atomique des surfaces d'alumine-γ était requise pour voir émerger de nouveaux concepts dans les catalyseurs supportés. Deux défis scientifiques majeurs ont été récemment relevés grâce aux approches modernes de la théorie de la fonctionnelle de la densité (DFT).

Le premier défi rapporté dans cette publication montre comment les simulations DFT couplées à des modèles thermodynamiques simples fournissent un moyen élégant pour déterminer les espèces chimiques (groupes hydroxyles, sites de Lewis, etc.) stables en fonction des conditions réactionnelles. Les surfaces (100) et (110), majoritairement présentes sur les nano-cristallites d'alumine-γ, possèdent deux comportements distincts relatifs à leur état d'hydroxylation. Alors que la surface (110) conserve un fort degré d'hydroxylation à haute température, la surface (100) se déshydrate dès les basses températures.

Cette première étape accomplie, le second défi scientifique dans le domaine a pu être abordé : il s'agit de l'étude de l'interaction phase active/alumine-γ. Dans cette publication, nous nous focalisons sur l'étude récente de l'adsorption d'un atome de palladium (Pd_1) sur les deux surfaces d'alumine (100) et (110). La détermination par DFT des surfaces d'énergie potentielles (SEP) de l'atome de Pd sur alumine permet d'étudier la relation entre la structure locale de l'interface $Pd_1/\gamma\text{-}Al_2O_3$ et l'énergie du système. De plus, de nouveaux apports sur les processus de chimisorption et de diffusion de l'atome de Pd sur les deux surfaces sont fournis. Il apparaît ainsi que l'énergie d'adsorption et la mobilité du Pd est réduite lorsque le taux d'hydroxylation augmente, comme c'est le cas pour la surface (110). En conclusion, le rôle de l'hydroxylation est révélé par la simulation DFT et permet de fournir des pistes d'explications de certaines observations expérimentales disponibles.

Abstract — DFT Study of the Interaction of a single Palladium Atom with γ-Alumina Surfaces: the Role of Hydroxylation — *Considering the crucial role of the γ-alumina solid phase in heterogeneous catalysis as a support of numerous active phases, a revised and improved atomistic description of γ-alumina surfaces was mandatory to furnish new highlights in the field of γ-alumina supported catalysts. Two important scientific challenges in heterogeneous catalysis have recently been taken up by modern Density Functional Theory (DFT) simulations.*

The first challenge described in this paper is to show that DFT calculations combined with simple thermodynamic model provide an elegant way of determining the stable chemical species at the γ-alumina surface (such as hydroxyls or Lewis sites) as a function of reaction conditions. The (100) and (110) surfaces exposed mainly by the γ-alumina nanocrystallites exhibit two distinct behaviors regarding their hydroxylation states. The (110) surface maintains a high degree of hydroxyl coverage even at high temperature, whereas the (100) surface is dehydrated at low temperature.

This first important step being achieved, a second challenge in heterogeneous catalysis is the interaction of the active phase with γ-alumina. In the second part of this paper, we present the adsorption of a single palladium atoms (Pd_1) on the (100) and (110) γ-alumina surfaces. By determining the potential energy surface of Pd on γ-alumina, the relationship between structure and metal-oxide interaction energy at the interface is depicted. Furthermore, new insights are provided on the chemisorption and diffusion processes of Pd on the two surfaces. The adsorption energy and the hopping rate of Pd are strongly reduced when the hydroxyl coverage increases such as found on the (110) surface. As a consequence, the surface hydroxylation appears as a key parameter for understanding the active phase/support interaction and enables the interpretation of available experimental data.

INTRODUCTION

Within the context of stronger environmental constraints encouraging the production of ever cleaner fuels, γ-alumina appears as a key industrial material for numerous applications in refining and petrochemistry [1, 2]. It is used as a catalyst in the Claus process (converting H_2S into elementary sulfur), or more widely as a catalytic support favoring the dispersion of various types of active phases. It is the case for transition metal sulfide active phases used in hydrotreatment catalysts to remove the sulfur and nitrogen from the most refractory compounds in order to avoid SO_x or NO_x emissions. γ-Alumina-supported Pt-Re catalysts are used for activating the formation of aromatics molecules from linear hydrocarbons in reforming processes. In petrochemistry, alumina-supported Pd catalysts selectively hydrogenate diolefins such as butadiene into butenes. These numerous examples involving γ-alumina in heterogeneous catalysis clearly put forward the two main challenges where *ab initio* molecular modeling can play a key role. The first one is to propose an accurate atomistic description of the γ-alumina surfaces in various experimental conditions of temperature and pressure of H_2O, H_2S, H_2, etc. The second one is to provide a better understanding of the active phase–support interaction. Providing new insights and concepts in these two areas is certainly helpful for a better control of the catalytic activity.

Investigating the physico-chemical properties of oxide surfaces is a rather complex task requiring the consideration of multiple phenomenon [3, 4] such as surface reconstruction, the polar character of the surface, and, moreover, the effect of the environmental conditions on the stability of surface species (Lewis sites, Brønsted sites, etc.). Furthermore, γ-alumina nanocrystallites used as a support in heterogeneous catalysts exhibit nano-scale sizes and specific morphologies with non-equivalent crystallographic surfaces. It is thus required to investigate the various atomistic and electronic properties of each exposed surface to understand the chemical properties of the catalyst. Since the pioneering work of Lippens and de Boer [5], γ-alumina surfaces have been extensively studied by nuclear magnetic resonance (NMR) [6-8], vibrational spectroscopies [9-12], or electron energy loss spectroscopy (EELS) [13]. Even if these experimental techniques have considerably improved the understanding and description of the γ-alumina properties, they seem to have reached some limits in furnishing unambiguous insights into the atomistic characterization of surface species. For instance, the nature of the surface hydroxyl groups and their relative concentrations are crucial to the understanding of acid-base properties. Infra-red (IR) spectra reveal up to seven different OH stretching bands [14], and proton NMR experiments show two distinct peaks for pure alumina and five peaks for deuterated samples [15]. The spectroscopic properties of the surface OH groups depend on their local environment: the number of Al atoms surrounding the hydroxyl groups, the local coordination of Al atoms, the possible existence of defects, etc. Before the advance of first principles simulation *(vide infra)*, the most popular empirical model of assignment of IR bands, given by Knözinger and Ratnasamy [11], was based on an empirical estimate of the "net electric charge", although it was questioned by experimental investigations [14, 16].

During the last twenty years, first principles (also called ab initio) simulations have brought key insights to the investigation of oxide surface properties. The methodology, based on the density functional theory (DFT) [17, 18] and implemented in efficient software [19-21], has made it possible to determine fundamental properties such as interatomic distances, local environment, vibrational properties, electronic properties of the valence band and core level. Some of these properties can be directly confronted with experimental characterization: extended X-ray absorption fine structure (EXAFS), X-ray photoelectron spectroscopy (XPS), infra-red spectroscopy (IR), etc. Recent studies [22, 23] illustrate the

high potential of combining experimentation and theory in order to make new progress in the knowledge of γ-alumina surfaces, where experimentation may have reached its limit.

As will be shown in this review, it is crucial to consider the effect of the experimental conditions (partial pressure of reactants and temperature) in order to determine the chemical termination of the surface, which is thermodynamically stable. The first part will thus be devoted to the first challenge in this area: to explain how DFT simulations have accomplished a step forward for understanding of the atomistic properties of γ-alumina surfaces. Relevant similar examples showing the evolution of the surface properties of various oxides in various conditions are well documented in the literature: RuO_2 [24], anatase-TiO_2 [25], MgO [26] and boehmite-AlOOH [27]. The reader can also refer to the recent review illustrating various DFT studies of fluid-mineral interactions at the molecular level [28], illustrating that the approach described in the present paper is rather general and can be applied to a wide range of materials (beyond heterogeneous catalysts).

The second challenge is to understand how the γ-alumina surface properties may impact the interaction with the active phase of the catalyst. This paper focuses on the metallic active phase. Other examples dealing with sulfide-γ-alumina interaction can be found in the literature [29]. The interaction of the support with the active phases plays an important role in the activity of the final catalysts [30]. A recent review by Henry [31] highlights the support effects on the structural and electronic properties of metallic active phases. STM experiments on Rh particles supported on a thin alumina film also revealed how the nucleation and dispersion of metal particles may change with the hydroxylation of the alumina film [32, 33]. Hence, the hydroxylation state of the support again appears as a key parameter.

As shown in this paper, DFT calculations become an important tool for exploring the effect of hydroxylation of γ-alumina surfaces on their interaction with a palladium atom [34]. Among recent works studying the interaction of palladium with model aluminum oxide surfaces, Márquez and Sanz have studied the interaction of Pd with a spinel-based model of γ-alumina [35]. Gomes *et al*. have studied the interaction of Pd atoms and small clusters with the γ-alumina (0001) surface [36-39]. Bogicevic and Jennison have characterized the interaction of a large group of metal adsorbates with aluminum oxide [40]. These works tend to emphasize that the interaction of Pd with aluminum oxide surfaces is correlated with the adsorbate's polarizability.

However, to our knowledge, little attention has been paid to two aspects: the influence of hydroxyl groups on metal-support interaction and the diffusion properties of metal adsorbates. Indeed, surface models in the absence of hydroxyls have been considered so far, whereas it is well known that under realistic conditions, the surface is populated by hydroxyl groups depending on the pre-treatment temperature. The influence of these OH groups on the metal surface interaction is a subject of fundamental and practical importance. This aspect will be discussed in the second part of the paper.

1 THE FIRST CHALLENGE: γ-ALUMINA SURFACES IN REACTION CONDITIONS

1.1 From Boehmite to γ-Alumina

γ-Alumina is a metastable transition alumina obtained by calcination of its hydrated precursor, boehmite γ-AlOOH at 700 K. The bulk model used in this study is taken from previous theoretical investigation of the calcination of boehmite [41]. Starting from the layered structure of boehmite, the dehydration process leads to the collapse of the boehmite sheets along the *y* axis, together with shearing along the *z* axis (see *Fig. 1*). The resulting structure exhibits an oxygen atom *fcc* sublattice, observed by XRD analysis [42]. This sublattice generates octahedral and tetrahedral interstices, to which aluminum atoms can diffuse. Compared with the model proposed in [42], a spinel-based structure arbitrarily imposes constraints on the type and number of interstices occupied by aluminum atoms. However, in order to achieve a Rietveld refinement [42], extra-spinel sites for aluminum atoms must be assumed, as in the most stable structures determined by DFT calculations [41-43]. In particular, it is shown that the cation positions (expressed in the $Fd\bar{3}m$ symmetry) are of spinel type 8a and of non-spinel type 48f for the tetrahedral sites, and of non-spinel type 16c and of spinel type 16d for the octahedral sites. More recent experimental neutron diffraction and theoretical investigations have confirmed this result [44].

The complete crystallographic structure and some important bulk properties compared with the experimental data are reported in [23], where a wide range of structural parameters are found, close to the experimental ones: the cell volume, the bulk modulus and the percentage of aluminum atoms in tetrahedral sites (25%), determined by NMR measurements. The simulated XRD diagram is also consistent with the experimental one. The model reproduces the tetrahedral distortion of the γ-alumina cell (inherited from the boehmite cell) [45].

1.2 From γ-Alumina Bulk to γ-Alumina Surfaces

1.2.1 General Considerations on Morphologies

Further considerations on γ-Al_2O_3 nanocrystallite morphology are useful, to justify the choice for the exposed crystallographic surfaces. The morphology of γ-alumina nanocrystallites strongly depends on the synthesis pathway. The standard method for producing γ-alumina is the precipitation of aluminum salts in an aqueous mother solution [2]: the formed

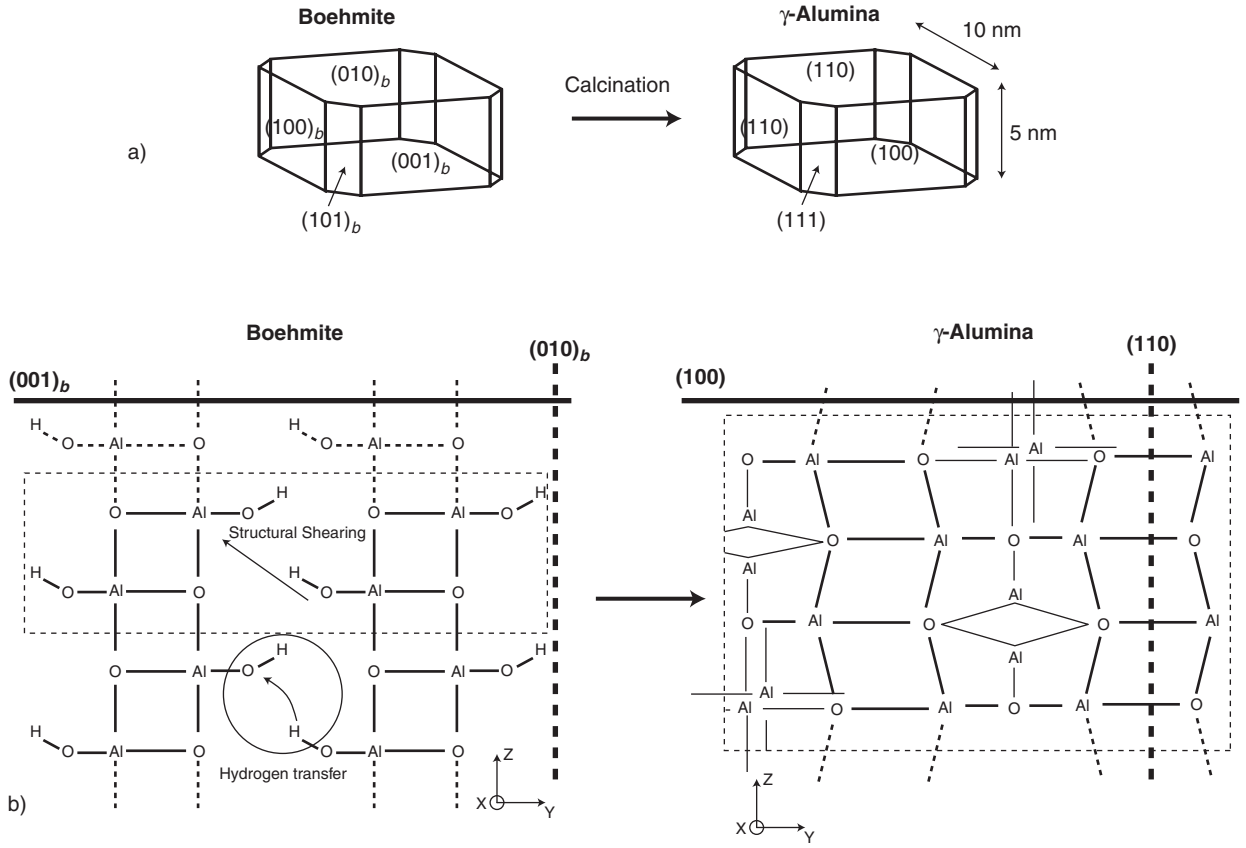


Figure 1

Topotactic transformation of the nanocrystallites of boehmite into γ-alumina with the corresponding crystallographic planes (a). Schematic bulk structures of boehmite and γ-alumina (b). The axes correspond to the boehmite orientation.

product is boehmite (γ-AlOOH), the hydrated precursor. Boehmite powders are calcinated at 700 K to recover γ-alumina. During the calcination process, water is released. The transformation is topotactic, meaning that the nanocrystallite morphology remains unchanged. This important characteristic is supported by TEM observations [46] and X-ray diffraction data [2].

The γ-alumina nanocrystallite morphology is thus directly inherited from the equilibrium morphology of boehmite nanocrystallites in an aqueous solution [27]. The most common shape of a boehmite nanocrystallite is rhombohedral: the predominant $(010)_b$ surface is referred as the basal surface, while three edge surfaces, $(100)_b$, $(001)_b$ and $(101)_b$, may be exposed *(Fig. 1a)*. The crystallographic analysis of the topotactic transformation reveals the relationship between boehmite surfaces and γ-alumina surfaces, as indicated in Figure 1. Using a spinel type indexation, the crystallographic nature of γ-alumina surfaces depends on the *fcc* oxygen atom sublattice: the (100) surface exhibits a square oxygen atom sublattice, the (110) a rectangular one and the (111) a hexagonal one. According to the pseudomorphism rules, the $(010)_b$ basal surface and the $(100)_b$ edge surface of boehmite yield the same type of surface, indexed as (110) in γ-alumina. The lateral $(001)_b$ and $(101)_b$ surfaces of boehmite correspond to the (100) and (111) surfaces, respectively. The modifications of the lattice parameters during the transformation of boehmite into γ-alumina are well reproduced by the calculation (as shown in [23, 41]). The rhombohedral shape is not modified, and the relative areas of the different surfaces do not greatly change, justifying the topotactic character of the transformation. Finally, in γ-alumina, the (110) surface predominates with 74% of the total area, followed by the (100) surface (16%) and the (111) surface (10%). These theoretical predictions are in good agreement with experimental results such as neutron diffraction analysis [47] or electron microscopy [46]. In what follows, we focus on the (110) and (100) surfaces. Specific results on the (111) surface can be found in [23].

1.2.2 Thermo-Chemistry of γ-Alumina Surfaces

Stoichiometric and fully dehydrated *(hkl)* surfaces are generated by cleaving the bulk structure *(Fig. 1b)* along the

plane defined by the *(hkl)* Miller indexes. For each surface, different terminations were tested, taking into account various distributions of surface atoms. The structures with the lowest surface energy are considered to be the most representative of the dehydrated surfaces.

The (de)hydration process of the oriented surfaces is described by the following equilibrium:

$$\gamma\text{-}Al_2O_{3(hkl)} + n_{ads}\, H_2O_{gas} \leftrightarrow \gamma\text{-}Al_2O_{3(hkl)} - n_{ads}\, H_2O_{ads} \quad (1)$$

where n_{ads} stands for the number of adsorbed water molecules per surface unit cell.

As explained in [22, 23], the Gibbs free energy associated with the reaction (1) is:

$$\Delta_r G\,(T, P, n_{ads}) = G(\gamma\text{-}Al_2O_{3(hkl)} - n_{ads}\, H_2O_{ads}) - G(\gamma\text{-}Al_2O_{3(hkl)}) - n_{ads}\, \mu_{H_2O} \quad (2)$$

where μ_{H_2O} is the chemical potential of water in the gas phase depending on T and P.

For a gas-phase molecule, the chemical potential is derived by density functional theory (DFT) calculations including the contribution of the partition functions for translation and rotation.

Some assumptions are required to calculate the Gibbs free energies of surfaces with various degrees of hydration, *i.e.* $G(\gamma\text{-}Al_2O_{3(hkl)} - n_{ads}\, H_2O) - G(\gamma\text{-}Al_2O_{3(hkl)})$. Calculating entropic and temperature dependencies of enthalpies of surfaces requires tremendous effort, such as determination of the vibrational modes of the surfaces. One approximation is to assume that $G(\gamma\text{-}Al_2O_{3(hkl)} - n_{ads}\, H_2O) - G(\gamma\text{-}Al_2O_{3(hkl)})$ is equal to $E(\gamma\text{-}Al_2O_{3(hkl)} + n_{ads}\, H_2O) - E(\gamma\text{-}Al_2O_{3(hkl)})$, where E is the internal energy of the surface at 0 K. This means that the variation in enthalpy and entropy contributions in $G(\gamma\text{-}Al_2O_{3(hkl)} - n_{ads}\, H_2O)$ and $G(\gamma\text{-}Al_2O_{3(hkl)})$ remains negligible versus variations in the chemical potential of water in the gas phase (included in μ_{H2O}). This assumption remains reasonable for medium or low hydroxyl coverage, as relevant for the current studies. For high hydroxyl contents, various hydroxyl configurations (close in energy) may co-exist. Temperature effects may also contribute to enhancing the proton and hydroxyl mobility at the surface. Without further insights into such subtle effects, one suggests choosing the surface state given by its lowest internal energy.

The values of E are calculated using density functional theory (DFT) as implemented in the Vienna Ab initio Simulation Package (VASP) [19-21]. VASP enables the determination of the one electron wave functions of the Kohn-Sham Hamiltonian, expanded in a plane wave basis set. The surface is modeled using periodic boundary conditions applied to supercells containing a "slab" of alumina. The self-consistent electronic energy is obtained with an iterative matrix diagonalization scheme, based on an unconstrained band-by-band residuum minimization method. For each cell configuration, atomic forces are calculated by means of the Hellmann-Feynman theorem, and the geometry optimization is performed with a conjugate-gradient algorithm. This means that for each hydration degree of the surface, the stable local structure of the surface is determined. The readers can find all important parameters used for the simulation in [22, 23].

Equation (2) can be rewritten to determine the surface energy of the *(hkl)* plane:

$$\Gamma_{hkl}\left(T, P, \theta_{hkl}\right) = \Gamma^0_{hkl} + \theta_{hkl}\Delta_r G\left(T, P, \theta_{hkl}\right) \quad (3)$$

where θ_{hkl} is the hydroxyl coverage of the *(hkl)* surface ($\theta_{hkl} = 2\, n_{ads} / A_{hkl}$ with A_{hkl} the surface area of the simulation cell), expressed in OH/nm^2. Γ^0_{hkl} represents the surface energy of the *(hkl)* plane of the reference surface.

It is thus possible to determine Γ_{hkl} as a function of P, T and n_{ads}. For a given value of P and T, the n_{ads} giving the lowest value of Γ_{hkl} corresponds to the thermodynamically stable surface, *i.e.* the most relevant one.

1.2.3 Stable Species on γ-Alumina Surfaces

Starting from the dehydrated surface, obtained by cutting the bulk structure along the (110) and (100) planes, an increasing number, n_{ads}, of water molecules is adsorbed. Different adsorption modes are tested: non-dissociative and dissociative modes. The reactivity of the different unsaturated aluminum sites present on these two surfaces are thus explored. The local structures of the two dehydrated surfaces are given in Figure 2. The coordination of the unsaturated aluminum atoms on the two surfaces varies from 3 to 5 (whereas in the bulk it is 4 or 6). As shown in [22, 23], the adsorption energy of water on the (100) surface as a function of the hydroxyl coverage decreases slightly from 105 to 65 kJ/mol. Indeed, the unsaturated aluminum atoms, being all of Al_V type, exhibit similar strength.

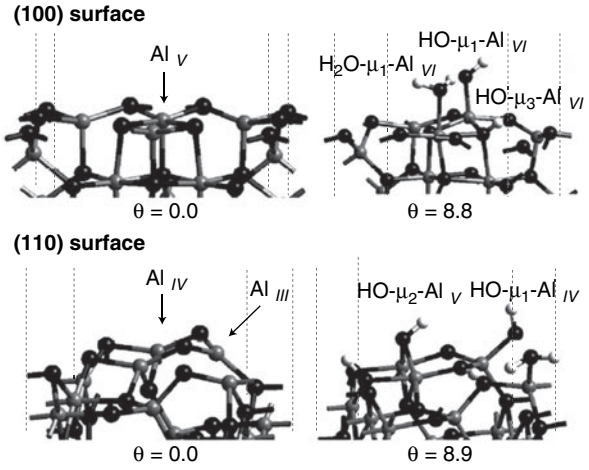


Figure 2

Local structures of the (100) and (110) γ-alumina surfaces for relevant hydroxyl coverages (θ).

In contrast, the adsorption energy on the (110) surface strongly depends on the hydroxyl coverage, decreasing from 240 to 87 kJ/mol. The first adsorption is dissociative and occurs on the Al_{III} site and on the adjacent μ_2-O site. The high exothermicity of this process (240 kJ/mol) can thus be explained by the strong intrinsic Lewis acidity of the highly unsaturated Al_{III} site. When increasing the OH-coverage, θ_{110}, the adsorption energies are reduced down to 88 kJ/mol. Due to the different local environments of the Al and O surface atoms, the (110) surface exhibits a larger range of adsorption energies and a greater variety of surface hydroxyl groups. The local structures of the hydrated surfaces are given in Figure 2.

The surface energy diagrams deduced from the adsorption energies of water are reported in Figure 3 for the (100) and (110) surfaces. According to the calculated surface energy values at the usual calcination temperature, we suggest that the observed morphology for γ-alumina nanocrystallites produced from boehmite calcination is metastable and imposed by the morphology of the boehmite precursor due to kinetic limitations. This interpretation justifies the topotactic transformation. We cannot exclude that other synthesis pathways may bypass such kinetic limitations and lead to different morphologies.

These diagrams also reveal the distinct behaviors of the two surfaces as a function of temperature. For temperatures greater than 600 K (at = 1 atm), the (100) surface is fully dehydrated (θ_{100} = 0 OH/nm^2). In contrast, the (110) surface remains hydrated up to high temperatures. This result is crucial for understanding the acid-base properties of the surfaces. In realistic conditions, the (100) surface exhibits mainly a great majority of Lewis aluminum sites, whereas the (110) surfaces exhibits a Brønsted acidity due to the hydroxyls. In particular, the validity of the hydroxylated surface models is further demonstrated by a careful comparison between OH stretching vibrational calculations and IR experiments (see *Table 1*). This leads to a revised assignment of the earlier Knözinger's proposal [11]. For a detailed analysis of these properties, the reader can refer to [22, 23].

Having established the two surface models, the second part of the paper focuses on the influence of the hydroxylation state on the interaction with palladium atoms.

TABLE 1

Calculated vibrational stretching frequencies of γ-Alumina surface hydroxyl groups. The site notation corresponds to the one used in Figure 2 and in the text

(details about OH stretching frequency calculations including anharmonic corrections are given in [22, 23, 27])

Site	Surface	ω_{calc} (cm^{-1})	ω_{exp} (cm^{-1})
HO-μ_1-Al_{IV}	(110)	3842	3785-3800
HO-μ_1-Al_{VI}	(100)	3777	3760-3780
HO-μ_1-Al_V	(110)	3736	3730-3735
HO-μ_2-Al_V	(110)	3707	3690-3710
HO-μ_3-Al_{VI}	(100)	3589	3590-3650

2 THE SECOND CHALLENGE: INTERACTION OF PALLADIUM WITH γ–ALUMINA SURFACES

2.1 The Potential Energy Surface (PES) of Pd

We should first bear in mind that, according to Section 1, the dehydrated γ-alumina (100) surface and the hydrated surface at OH coverage of 11.8 OH/nm^2 for temperatures close to

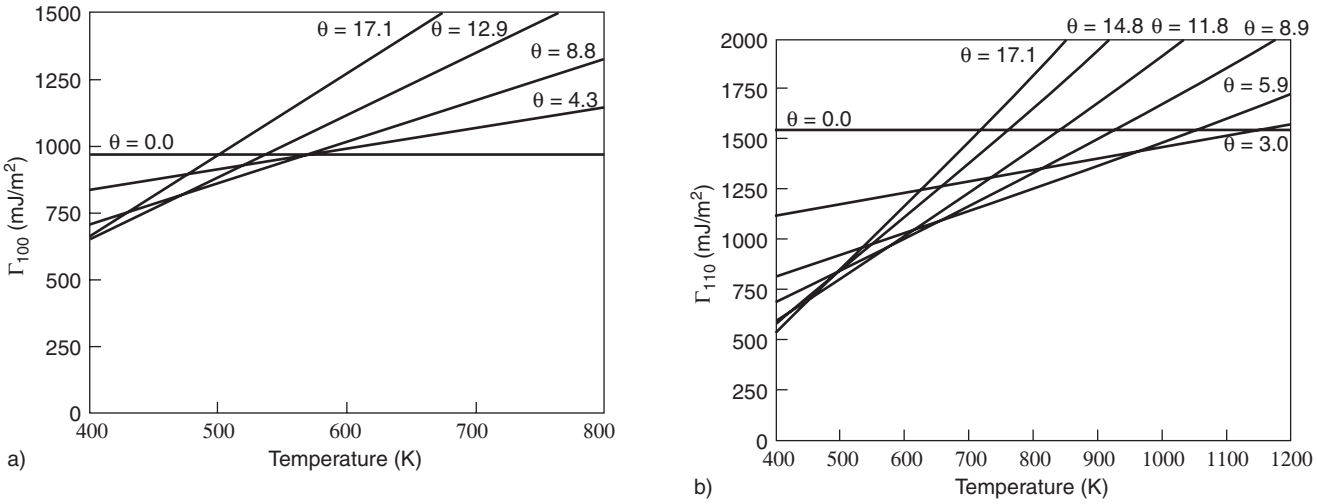


Figure 3

Surface energy as a function of temperature (for standard pressure) and various hydroxyl coverages (θ) for the (100) γ-alumina surface (a) and the (110) surface (b).

600 K. Supported catalysts prepared by an ion-exchange process are usually calcined and reduced at such temperature. We presume that Pd precursors lose their ligands after calcination and Pd atoms become Pd^0 at the end of the reduction step. To investigate the interaction of palladium atoms with the γ-aluminum surfaces, an elegant way is to determine the so-called potential energy surface (PES) of one palladium atom on the (100) and (110) γ-alumina surfaces. As previously underlined, it is required to consider the stable hydroxylation state of the surface according to the temperature. The (100) surface is completely dehydroxylated, whereas the (110) surface contains 11.8 OH/nm^2. The fully dehydrated (110) surface was also considered, even if it does not exist in this temperature range and water pressure atmosphere, since it provides a direct analysis of hydration effect. Besides, even if this low hydration state is beyond real experimental conditions, it mimics surface sites with a high degree of unsaturation, such as defective sites.

In order to construct the PES, the palladium atom is displaced on a grid of points sampling the surfaces. Each point represents a surface area of 1.1 Å^2. For each position of the palladium atom, a constrained geometry optimization is performed. All atoms' degrees of freedom of the γ-alumina cell are allowed to change. For the palladium adsorbate, the coordinates parallel to the surface plane (x_0,y_0) are kept fixed at each grid point and only the coordinate in the direction perpendicular to the surface (z) is allowed to relax. This sampling provides a set of adsorption energies associated with a position in the atomistic model. Therefore, the interaction energy values as a function of the position are defined as:

$$E_{ads}(Pd_1/\gamma\text{-}Al_2O_{3\,(hkl)})(x_0, y_0, z) = E(Pd_1/\gamma\text{-}Al_2O_{3\,(hkl)})(x_0, y_0, z) - E(Pd_1) - E(\gamma - Al_2O_{3\,(hkl)}) \quad (4)$$

As in paragraph 1.2.2, E represents the internal energies of the systems: it is thus calculated using the same DFT approach as described in the first part. $E(Pd_1)$ and $E(\gamma\text{-}Al_2O_{3(hkl)})$ are the reference energy for the isolated palladium atom and the γ-alumina *(hkl)* surface. The PES are visualized by maps *(Figs. 4 and 5)* representing the variation in E_{ads} as a function of (x, y) on the surface.

2.2 Adsorption of Palladium on the γ-Alumina Surfaces

2.2.1 Adsorption on the (100) γ-Alumina Surface

The local structure of the surface is described in detail in paragraph 1.2.2. The computed PES reveals that adsorption energies are in a range from –0.4 to –1.4 eV *(Fig. 4a)* . The superposition of the surface atomistic model on the PES shows that the regions of the strongest metal-surface interaction are in the vicinity of the penta-coordinated aluminum atoms, whereas those of weakest interaction are on the tetrahedral sub-surface atoms. The structure and energetics analysis reveals that the most favorable site on this surface is made of an Al-Pd-O bridge. The structure of the stable $Pd_1/\gamma\text{-}Al_2O_{3(100)}$ complex for this site *(Fig. 4b)*, reveals that some surface Al-O bonds with Al and O atoms involved in the interaction with Pd are weakened, whereas other Al-O bonds are strengthened following a bond order conservation principle. These results underline the important contribution of surface relaxation to adsorption energies. Our calculations reveal that the surface relaxation energy contributes up to 25% of Pd adsorption energies. The $\gamma\text{-}Al_2O_3$ (100) surface is hence not static during Pd adsorption. In contrast, the surface adapts itself to optimize the Pd-surface bonding by reorganization of the Al-O bond strengths. Adsorbate-induced surface relaxation has also been observed in other aluminum oxide

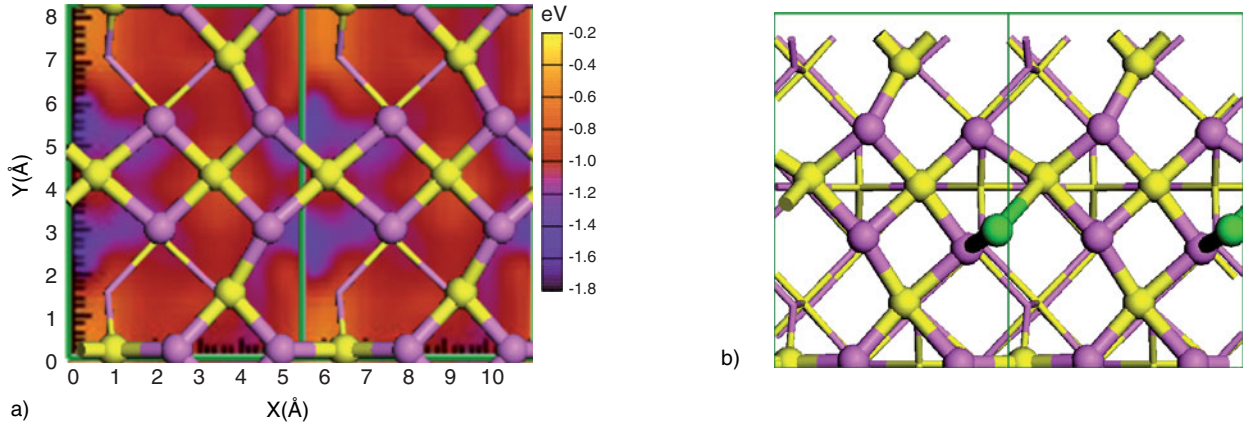


Figure 4

(2 × 1) view of the potential energy surface (PES) of the palladium atom on the (100) surface of γ-alumina (a). Local structure of the palladium atom adsorbed on the most favored position of the PES (b). Violet balls: O; yellow balls: Al; green atoms: Pd.

polymorphs such as γ-Al_2O_3, with a similar contribution to adhesion energies [37]. Including surface relaxation in the calculation model is thus required for a correct description of the metal-oxide interaction.

2.2.2 Adsorption on the (110) γ-Alumina Surface

This surface is extremely corrugated and the presence of unsaturated aluminum atoms makes this surface very reactive. As explained in paragraph 1.2.3, the surface is hydrated even after a treatment at high temperatures (a temperature higher than 1200 K is required for complete dehydration). According to the first part of this review, this surface contains 11.8 OH/nm^2 at 600 K and normal water pressure.

The computed PES for the dehydrated and hydrated γ-Al_2O_3 (110) surfaces are shown in Figures 5a and 5b, respectively. Interaction energies for the dehydrated surface vary from –1.0 eV to –1.7 eV. The more open nature of the (110) surface intrinsically tends to favor sites with engaged multiple bonds with Pd. The strongest binding site is in the vicinity of the Al_{III} site, which exhibits the highest unsaturation, and the adsorption structure after complete optimization is depicted in Figure 5 c. The Pd-O bond length on the dehydrated (110) surface is 0.03 Å smaller than the Pd-O bond found on the (100) surface, which seems to be reasonable since the former surface O atom has a lower coordination number and favors a stronger bonding.

On the other hand, adhesion energies are reduced for the hydrated γ-Al_2O_3 surface and vary from –0.2 eV to –1.4 eV. The dissociative adsorption of water decreases the Lewis acidity of the Al surface atoms and the Lewis basicity of the O surface atoms. The stable adsorption site of the dehydrated surface is completely changed since the Al site is saturated by an OH group, while the vicinal oxygen atoms are baring a proton. The strongest binding site for the hydrated surface exhibits multiple bonding between palladium and two μ_1-OH sites, one Al_{VI} aluminum and a weak interaction with the proton of the μ_3-OH group *(Fig. 5d)*.

Similar to the (100) surface, the contribution of surface relaxation to adhesion energies for the (110) surface can reach up to 45% of the interaction energy on the dehydrated surface, and up to 70% on the hydrated one. The fact that the (110) surface is more corrugated reveals a larger capability to adapt its structure to Pd adsorption compared with the (100) one. The great contribution of surface relaxation to adsorption energies in the case of the hydrated surface can be understood by the rotational flexibility of its hydroxyl groups.

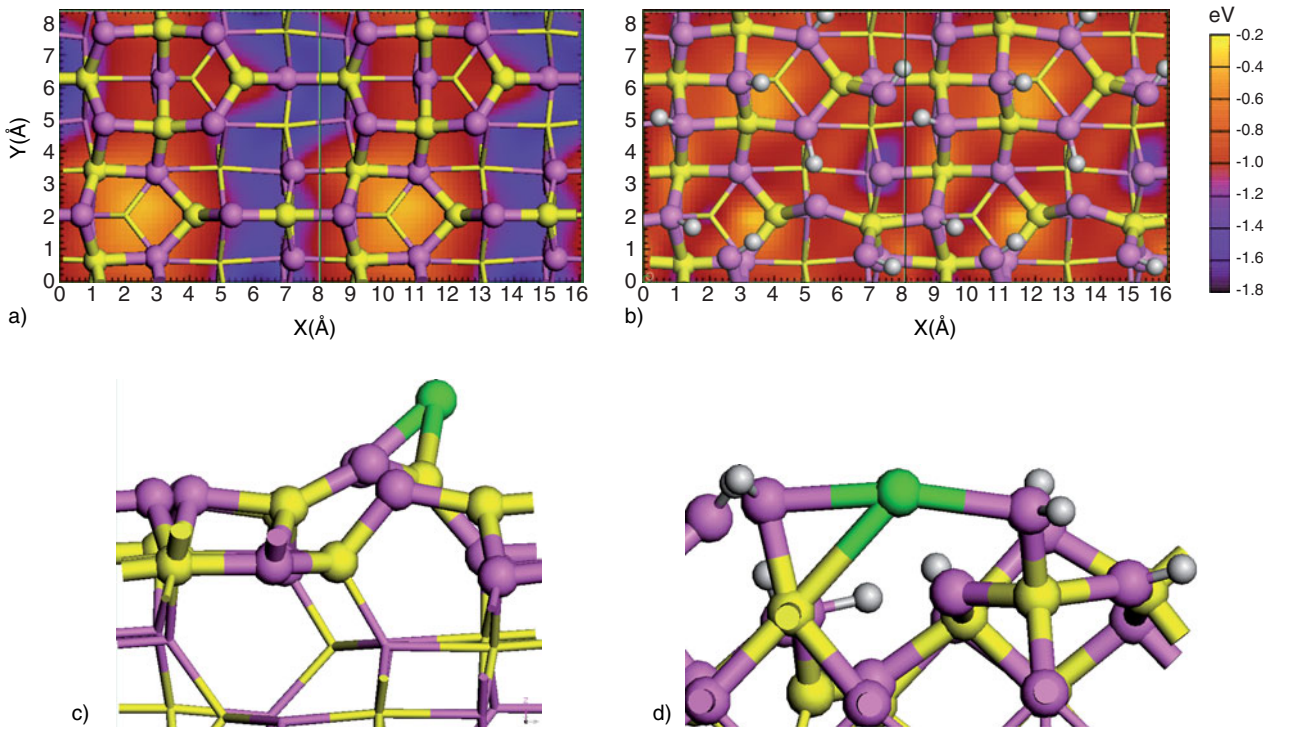


Figure 5

(2 × 1) view of the potential energy surface (PES) of the palladium atom on the (110) surface of γ-alumina (a) dehydrated (b) hydrated. Local structure of the palladium atom adsorbed on the energetically favored position of the PES (c) dehydrated (d) hydrated. Violet balls: O; yellow balls: Al; green atoms: Pd; white balls: H.

2.3 Diffusion Properties of Palladium on the γ-alumina Surface

The low energy diffusion paths of Pd ad-atoms are determined on the γ-alumina surfaces and their energy barriers from the computed PES. According to transition state theory, the mean number of diffusion events per second between two sites, also known as the "hopping rate", is given by the following equation:

$$\eta = \upsilon \exp\left(\frac{-\Delta E}{k_B T}\right) \quad (5)$$

where v is a typical oscillation frequency and ΔE the energy barrier between two sites. An estimation of the hopping rate between sites at the dwell of each computed PES is obtained by considering the trajectories of the smallest ΔE and a standard value of 6.10^{12} s^{-1} for v in Equation (5). We considered for each surface two possible trajectories: the first one parallel to the X direction and the second one parallel to the Y direction. The trajectories for the (100) surface are shown in Figure 6. The energy barriers are thus deduced, and the temperature dependences of η are given in Figure 7.

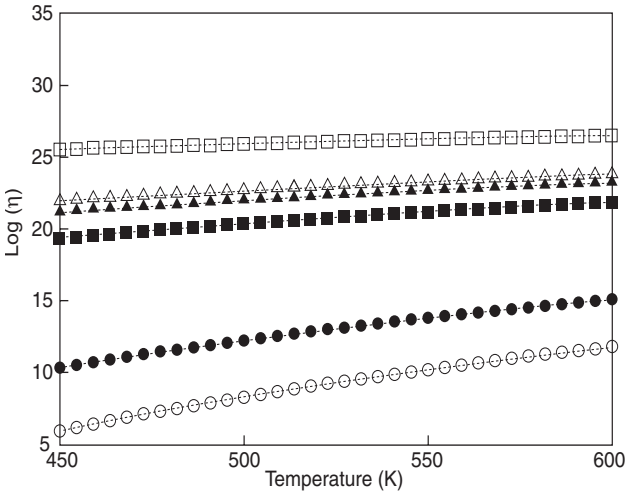


Figure 7

Temperature dependence of the hopping rates, η (see text for definition), of palladium on the γ-alumina surfaces: filled triangle: (100) X direction, empty triangle: (100) Y direction, filled square: dehydrated (110) X direction, empty square: dehydrated (110) Y direction, filled circle: hydrated (110) X direction, empty circle: hydrated (110) Y direction.

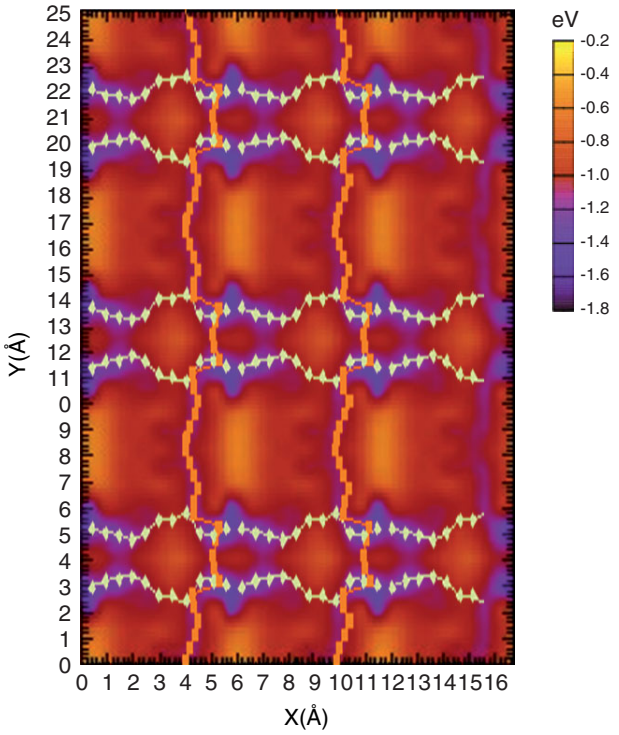


Figure 6

(3 × 3) view of the two low energy diffusion trajectories (along X and Y axes) of the palladium atom on the γ-alumina (100) surface.

Figures 6 and 7 show that Pd has a high degree of mobility along the rows of surface Al_V atoms on the (100) orientation of alumina. Besides, the energy barriers for the two considered trajectories are very similar. Therefore, Pd atoms can move along the X and Y directions with almost equal probability.

As for the dehydrated (110) surface, Figure 7 shows that diffusion is more favorable along the Y direction, where Pd interacts with the surface unsaturated Al_{IV} and Al_{III} species, than along the X direction. This could be explained by the fact that the other surface aluminum atoms of the (110) orientation are in hindered positions. The hopping rates at 473 K for the *X* and *Y* directions are close and remain very high.

In contrast, Figure 7 shows a sharp decrease in the hopping rate of this orientation when it is hydrated. The most favored site represents a deep potential dwell where the metal atom is trapped by strong interactions with two surface hydroxyl groups of μ_1-type and one cooperative Al atom (see *Fig. 5d*). As indicated earlier, the neighboring species on the surface are μ_2- and μ_3-OH groups, with less accessible O atoms and weakly interacting H atoms. Therefore, a large diffusion barrier of +0.8 eV results for this hydrated surface.

Our results give a reasonable picture of the diffusional behavior of Pd on γ-alumina and they also help to understand the initial steps of nucleation on the exposed surfaces at 473 K. On the hydrated surface, nucleation takes place in trapping sites for Pd atoms with significant binding energies. The low mobility of Pd on this surface favors the formation

of a large number of small sized clusters. The mobility of Pd in both dehydrated (110) and (100) surfaces is high and Pd-surface binding energies are small compared with the cohesion energy of Pd in the bulk. Therefore, we should expect this adsorbate to form larger particles on the dehydrated (110) and (100) surfaces. The preparation of the alumina and its surface termination support should then have an influence on the structure of the Pd deposited particles.

This dependence of the palladium atoms' mobility on the hydroxylation state may explain experimental results [48] showing that the size of the Pd particles formed on the γ-alumina surfaces increases as the temperature of reduction increases: a combined effect of dehydration and temperature-driven sintering. Our results could highlight the role of hydroxylation in preventing the sintering of supported Pd particles.

On the basis of our simulation, we propose a consistent explanation of the STM experiments on thin alumina film-supported Rh particles [32, 33], assuming reasonably that our results obtained on Pd are transferable to Rh. They have observed that hydroxylation decreases the size of nucleated metal particles and increases their dispersion. Although the ultrathin alumina film structure used in experiments differs from γ-alumina, we suggest that the film hydroxylation reduces the diffusion properties of Rh metal atoms, which may explain the better dispersion of Rh metal particles as observed by STM.

Recent results highlight the relevance of defect sites in the nucleation of Pd dimers in the MgO(100) surface [49]. Our results for the dehydrated (110) surface can be regarded as a model for multiple defect points. The low coordination number of Al and O atoms present on the dehydrated (110) surface could mimic local defects (regions where water molecules are absent, or steps with low coordination numbers). Such regions exhibit significantly higher adsorption energies for Pd than hydrated regions of either the (110) or (100) surfaces. These defective regions can be favorable for Pd nucleation (as proposed by the latter reference).

CONCLUSION

DFT investigations of the dehydration process of boehmite into γ-alumina, which is the industrial way of producing γ-alumina, found a new bulk model for γ-alumina. As confirmed by several theoretical calculations combined with XRD experiments, it was shown in particular that Al atoms also occupy non-spinel sites in the γ-alumina structure.

The use of DFT combined with a thermodynamic model has provided optimized models of γ-alumina surfaces under reaction conditions. Morphology and reaction conditions have a direct impact on the nature and concentration of the stable surface hydroxyl species, fundamental for a clear understanding of γ-alumina surface chemistry. The reliability of the surface models was tested against a wide list of available experimental data. Hence, this approach made it possible to significantly improve empirical models with strong limitations and allowed a step forward to a more rational understanding of γ-alumina acid-base properties.

Focusing on Pd_1/γ-alumina interaction, the potential energy surfaces (PES) of a single palladium ad-atom on the γ-alumina surfaces in standard reaction conditions has pointed out the dependence of interaction modes and energies on the selected surfaces. Above all, it is found that the surface hydroxylation decreases the adsorption energies of the palladium atom and its mobility as calculated by diffusion rate.

This work opens up new ways of investigating support effects as they occur in real industrial catalysts. A systematic comparison with another important oxide catalytic support, anatase-TiO_2, was also achieved more recently [25, 50]. We intend to investigate in the near future the interaction between Pd clusters of larger size with γ-alumina surfaces in order to explore the reactivity on even more realistic models of γ-alumina-supported metallic systems, with the ultimate goal for DFT simulation to become a tool for the rational design of future industrial catalysts.

ACKNOWLEDGEMENTS

The authors acknowledge H. Toulhoat from IFP for fruitful discussions. Manuel Corral Valero is grateful to IFP and ANRT for research grants.

REFERENCES

1 Ertl, G., Knözinger, H., Weitkamp, J. (1997) *The Handbook of Heterogeneous Catalysis*, Wiley-VCH, Weinheim.

2 Euzen, P., Raybaud, P., Krokidis, X., Toulhoat, H., Le Loarer, J.-L., Jolivet, J.-P., Froidefond, C. (2002) *Handbook of Porous Solids*, Vol. 3, Schüth, F., Sing, K.S.W., Weitkamp, J. (Eds.), Wiley-VCH Verlag GmbH, Weinheim, p. 1591.

3 Jolivet, J.-P. (1998) *De la solution à l'oxyde*, EDP Sciences, Paris.

4 Noguera, C. (1995) *Physique et chimie des surfaces d'oxydes*, Eyrolles, Paris.

5 Lippens, B.C., de Boer, J.H. (1964) *Acta Crystallogr.*, **17**, 1312.

6 Hietala, J., Root, A., Knuuttila, P. (1994) *J. Catal.*, **150**, 46.

7 Guillaume, D., Gautier, S., Alario, F., Devès, J.M. (1997) *Oil Gas Sci. Technol.*, **54** (4), 537.

8 Zhang, W., Sun, M., Prins, R. (2002) *J. Phys. Chem.*, **106**, 537.

9 Tsyganenko, A.A., Filimonov, V.N. (1973) *J. Mol. Struct.*, **19**, 579.

10 Morterra, C. (1988) *J. Chem. Soc. Farad. T. 1*, **84**, 1617.

11 Knözinger, H., Ratnasamy, P. (1978) *Catal. Rev.*, **17**, 31.

12 Saad, A.B. Mohammed, Ivano, V.A., Lavalley, J.C., Nortier, P., Luck, F. (1993) *Appl. Catal.*, **94**, 71.

13 Ealet, B., Elyakhlouffi, M.H., Gillet, E., Ricci, M. (1994) *Thin Solid Films*, **250**, 92.

14 Morterra, C., Magnacca, G. (1996) *Catal. Today*, **27**, 497.

15 De Canio, E.C., Edwards, J.C., Bruno, J.W. (1994) *J. Catal.*, **148**, 76.

16 Busca, G., Saussey, H., Saur, O., Lavalley, J-C., Lorenzelli, V. (1985) *Appl. Catal.*, **14**, 245.

17 Kohn, W., Sham, L. J. (1965) *Phys. Rev. A*, **140**, 1133.

18 Hohenberg, P., Kohn, W. (1964) *Phys. Rev. B*, **136**, 864.

19 Kresse, G., Furthmüller, J. (1996) *Comp. Mater. Sci.*, **6**, 15.

20 Kresse, G., Furthmüller, J. (1996) *Phys. Rev. B*, **54**, 11169.

21 VASP - the guide. http://cms.mpi.univie.ac.at/vasp/

22 Digne, M., Sautet, P., Raybaud, P., Euzen, P., Toulhoat, H. (2002) *J. Catal.*, **211**, 1.

23 Digne, M., Sautet, P., Raybaud, P., Euzen, P., Toulhoat, H. (2004) *J. Catal.*, **226**, 54.

24 Reuter, K. (2006) *Oil Gas Sci. Technol.*, **61**, 4, 471-477.

25 Arrouvel, C., Toulhoat, H., Breysse, M., Raybaud, P. (2004) *J. Catal.*, **226**, 260.

26 Ealet, B., Goniakowski, J., Finocchi, F. (2004) *Phys. Rev. B*, **69** (19), 195413.

27 Raybaud, P., Digne, M., Iftmie, R., Wellens, W., Euzen, P., Toulhoat, H. (2001) *J. Catal.*, **201**, 236.

28 Toulhoat, H., Digne, M., Arrouvel, C., Raybaud, P. (2005) *Oil Gas Sci. Technol.*, **60**, 417.

29 Arrouvel, C., Breysse, M., Toulhoat, H., Raybaud, P. (2005) *J. Catal.*, **232**, 161.

30 Argo, A.M., Odzak, J.F., Lai, F.S., Gates, B.C. (2002) *Nature*, **415**, 623.

31 Henry, C.R. (1998) *Surf. Sci. Rep.*, **31**, 231.

32 Heemeier, M., Frank, M., Libuda, J., Wolter, K., Kuhlenbeck, H., Bäumer, M., Freund, H.J. (2000) *Catal. Lett.*, **68**, 19.

33 Libuda, J., Frank, M., Sandell, A., Andersson, S., Bruhwiler, P.A., Bäumer, M., Martensson, N., Freund, H.J. (1997) *Surf. Sci.*, **384**, 106.

34 Corral Valero, M., Raybaud, P., Sautet, P. (2006) *J. Phys. Chem. B*, **110**, 1759.

35 Márquez, A.M., Sanz, J.F. (2004) *Appl. Surf. Sci.*, **238**, 82.

36 Gomes, J.R.B., Illas, F., Hernandez, N.C., Sanz, J.F. (2002) *Phys. Rev. B*, **65**, 125414.

37 Gomes, J.R.B., Illas, F., Hernandez, N.C., Sanz, J.F., Wander, A., Harrison, N.M. (2002) *J. Chem. Phys.*, **116**, 1684.

38 Gomes, J.R.B., Illas, F., Silvi, B. (1999) *Chem. Phys. Lett.*, **388**, 132.

39 Gomes, J.R.B., Lodziana, Z., Illas, F. (2003) *J. Phys. Chem. B*, **107**, 6411.

40 Bogicevic, A., Jennison, D.R. (1999) *Phys. Rev. Lett.*, **82**, 4050.

41 Krokidis, X., Raybaud, P., Gobichon, A-E., Rebours, B., Euzen, P., Toulhoat, H. (2001) *J. Phys. Chem. B*, **105**, 5121.

42 Zhou, R.S., Snyder, R.L. (1991) *Acta Crystallogr. B*, **47**, 617.

43 Wolverton, C., Haas, K.C. (2001) *Phys. Rev. B*, **63**, 024102.

44 Paglia, G., Rohl, A.L., Buckley, C.E., Gale, J.D. (2005) *Phys. Rev. B*, 71, 224115.

45 Wilson, J.C. (1979) *J. Solid State Chem.*, **30**, 247.

46 Nortier, P., Fourre, P., Saad, A.B. Mohammed, Saur, O., Lavalley, J.-C. (1990) *Appl. Catal.*, **61**, 141.

47 Beaufils, J.P., Barbaux, Y. (1981) *J. Chim. Phys.*, **78**, 347.

48 Sun, K., Liu, J., Nag, N., Browning, N.D. (2002) *Catal. Lett.*, **84**, 193.

49 Giordano, L., Di Valentin, C., Goniakowski, J., Pacchioni, G. (2004) *Phys. Rev. Lett.*, **92**, 096105.

50 Arrouvel, C., Digne, M., Breysse, M., Toulhoat, H., Raybaud, P. (2004) *J. Catal.*, **222**, 152.

Final manuscipt received in June 200

Copyright © 2006 Institut français du pétrole

Permission to make digital or hard copies of part or all of this work for personal or classroom use is granted without fee provided that copies are not made or distributed for profit or commercial advantage and that copies bear this notice and the full citation on the first page. Copyrights for components of this work owned by others than IFP must be honored. Abstracting with credit is permitted. To copy otherwise, to republish, to post on servers, or to redistribute to lists, requires prior specific permission and/or a fee: Request permission from Documentation, Institut français du pétrole, fax. +33 1 47 52 70 78, or revueogst@ifp.fr.